Electronic Supplementary Material (ESI) for Nanoscale.

Supplementary Material

Efficient single-photon pair generation by spontaneous parametric down-conversion in nonlinear plasmonic metasurfaces

Boyuan Jin, Dhananjay Mishra, and Christos Argyropoulos*
Department of Electrical and Computer Engineering, University of Nebraska-Lincoln, Lincoln, Nebraska 68588, USA
*christos.argyropoulos@unl.edu

1. Numerical method to simulate the linear response and nonlinear SFG process

In this work, the linear and nonlinear SFG processes are numerically modeled in the frequency domain by using COMSOL Multiphysics. COMSOL is a commercial simulation software based on the finite element method (FEM) and its RF module is used to carry out the presented full-wave electromagnetic simulations. These simulations are not trivial, since the COMSOL solver equations need to be substantially modified and customized to introduce the nonlinear response of the bulky material $LiNbO_3$ and metal-dielectric interface. More specifically, the second-order nonlinear response at the metal-dielectric interface is simplified and converted to a nonlinear surface current to reduce the computation load and accelerate the nonlinear simulations. More details about this part of the modeling will be provided later in this section. Similar simulation methods had been widely applied to numerically model various nonlinear optical effects, including SFG, based on plasmonic or dielectric structures and has been verified to accurately predict relevant various experimentally observed results.[1-5]

The proposed plasmonic metasurface (shown in Fig. 1 in the main paper) is composed of an array of silver nanostripes periodically placed on top of a dielectric spacer layer made of $LiNbO_3$. At the bottom, the substrate made of silver works as a perfect reflector and thus the plasmonic metasurface is working in the reflection mode. The silver nanostripes and substrate enhance the electric field distribution in the $LiNbO_3$ layer, as shown in Fig. 2b in the main paper. The proposed structures are uniform in the y-axis along the nanostripe direction, and therefore are simulated as two-dimensional (2D) systems. We also tried three-dimensional (3D) relevant simulations (not shown here), where it was verified that the results of the 2D model have great accuracy, but its calculations are less time consuming. Two ports are placed on the upper and bottom boundaries of the simulation domain operating at both incident wavelengths λ_1 and λ_2. Due to the periodicity of the structure, only one silver nanostripe needs to be included in the simulation domain and periodic boundary conditions are used in the left and right boundaries. The resulted input radiation is a typical plane wave source that propagates from the upper to the bottom port.

The linear permittivities of silver and $LiNbO_3$ are taken from experimental data.[6, 7]

During the SFG process in any nonlinear material, the incident waves operating at λ_1 and λ_2 can generate a new wave at the sum-frequency equal to λ_{SF}. The sum-frequency wave is generated by the nonlinear materials composing the relevant structure. Hence, the upper and bottom boundaries of the simulation domain are replaced by "passive" scattering boundaries to detect the generated wave at λ_{SF}. The nonlinear media in the plasmonic metasurface includes the $LiNbO_3$ dielectric layer and the silver-dielectric interfaces. The wave equation in frequency domain derived from Maxwell's equations is modified in the case of nonlinear simulations to:

$$\nabla \times (\mu_r^{-1} \nabla \times \mathbf{E}) - \varepsilon_r k_0^2 \mathbf{E} = \mu_0 \omega^2 \mathbf{P}^{NL} . \tag{1}$$

The non-zero term $\mu_0 \omega^2 \mathbf{P}^{NL}$ on the right side of this equation is added into COMSOL by using a weak-form partial differential equation (PDE) module, similar to previous simulations of various nonlinear metamaterials.[1-4, 8]

At the silver-dielectric interface, the second-order nonlinearity arises from the surface nonlinear susceptibilities: $\chi^{(2)}_{s\perp,Ag}$ and $\chi^{(2)}_{s\|,Ag}$, where $\chi^{(2)}_{s\|,Ag}$ is very weak and is neglected.[9-11] Computing the polarizability $\mathbf{P}^{NL}_{s\perp} = 2\varepsilon_0 \chi^{(2)}_{s\perp,Ag} E_{1\perp,Ag} E_{2\perp,Ag} \hat{\mathbf{r}}_\perp$ is tricky because COMSOL cannot deal with a surface current in the normal to surface direction. Many numerical methods have been implemented to overcome this difficulty, such as using the nonlinear Mie-type solutions,[12] the weak form of the differential equations,[13] and the surface integral method.[14] In this work, $\mathbf{P}^{NL}_{s\perp}$ is assumed to be equivalent to a surface magnetic current density given by the formula: $\mathbf{J}^{NL}_{m,s} = \hat{\mathbf{r}}_\perp \times (\nabla_\| P^{NL}_{s\perp}) / \varepsilon'$, similar to previous published works.[15] The surface magnetic current can be directly calculated by COMSOL, since it only contains tangential components. The x and z components of $\hat{\mathbf{r}}_\perp$ are denoted by n_x and n_z, respectively. The "down" and "up" functions are used to express the electric field in the silver surface, rather than in the adjacent dielectric media. Finally, the "dtang" function is used to obtain the gradient along the tangential surface.

As the SFG is a very weak process and the conversion efficiency CE_{SFG} is usually less than few percent, the power transferred to the sum-frequency is much lower than the incident wave powers at λ_1 and λ_2. Therefore, the undepleted-pump approximation is adopted throughout all our SFG calculations. The transmittance and reflectance at the incident wavelengths λ_1 and λ_2 are accurately computed by linear simulations without the need of adding extra nonlinear terms. Note that the computational burden and simulation time consumption is substantially lower in the case of linear modeling.

To calculate the SFG efficiencies CE_{SFG} and η_{SFG}, we need to measure P_{SF}, which is the reflected power at the sum-frequency. P_{SF} is computed by setting boundary probes on all the outer boundaries of the simulation domain and then integrating the power density outflow at the sum-frequency. Normal incident waves are used in this work and the incident powers are given by: $P_1 = I_1 a$ and $P_2 = I_2 a$, where a is the periodicity of the plasmonic metasurface. The Far-Field Domain module of COMSOL is used to calculate the near-to-far-field transformation of the computed at the near-field reflected power P_{SF} at the sum-frequency point. This calculation happens for one unit cell because the presented metasurface is periodic. The same far-field calculations have been used before to compute the directivity of a different nonlinear process (four-wave-mixing) boosted by a similar metasurface[16] with much smaller gap size. The resulted SFG radiation pattern of the metasurface is shown in Fig. 4 in the main paper, where it is proven that the optimum SFG performance occurs only for normal incidence illuminations.

Finally, very fine mesh is used in the simulation domain, especially in the $LiNbO_3$ layer, and at the corners and edges of the silver nanostripe. The minimum mesh size is equal to 0.5 nm < $10^{-3}\lambda_{SF}$. This fine mesh guarantees the accuracy of the nonlinear simulation results and can accurately deal with potential instabilities caused by the enhanced electric field in the plasmonic metasurface.

2. Plasmonic metasurface excited by circular polarized incident waves

In Fig. 5b in the main text, we compare the field enhancement between the linear and circular polarizations. The incident intensity in Fig. 5b is chosen to be very low and the plasmonic metasurface operation is in the linear regime. Here, the reflectance spectra induced by circular polarized excitations are also computed and shown in Fig. S1. Note that the reflectance spectrum under the O-polarized excitation is shown in Fig. 2a in the main text. Both LCP and RCP incident waves can generate a deeper reflectance dip accompanied by a slightly narrower bandwidth. On the other hand, the resonant wavelengths are almost unchanged to those in the case of linear polarization, suggesting the proposed plasmonic metasurface will enhance the nonlinear process in a similar way for circular polarized inputs, as was shown in the main text. Finally, it is worth noting that the reflection response is the same for both LCP and RCP incident waves since the structure is not chiral.

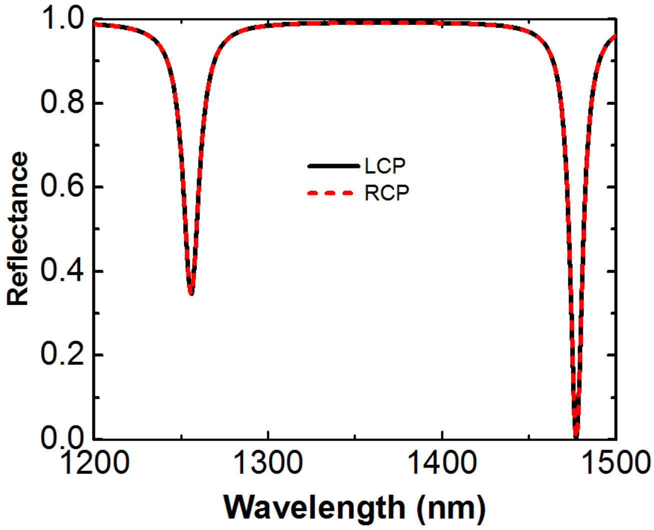

Fig. S1 Linear reflectance as a function of the wavelength when the incident light is circular polarized.

Interestingly, the reflectance is narrower and deeper in the case of circular polarization, as it is shown in Fig. S1. In addition, the field enhancement is higher in this case, as it is depicted in Fig. 5(b) in the main paper. This is the main cause of higher SFG conversion efficiency in the case of circular polarized incident waves with relevant results demonstrated in Fig. 5(a) in the main paper. Hence, it seems that stronger coupling exists between circular polarized excitation and the resonance modes of the presented plasmonic metasurface. In order to further understand this effect, the magnetic field distributions induced in the nanogap of the metasurface at the two reflectance resonances (1254 nm and 1479 nm) are plotted in Fig. S2, where it is demonstrated that both modes are of the same magnetic nature. Note that the electric field distributions of the same modes are shown in Fig. 2(b) in the main paper. It is interesting that the magnetic field is localized on the upper nanogap region in the 1479 nm resonance and on the lower nanogap region in the 1254 nm resonance. Magnetic modes are based on circulating electric fields and, as a result, can couple in a more efficient way to circular polarization, which is also the case in our design. Similar conclusions were derived in previous works that used the currently presented gap-plasmon metasurface mainly as polarizer.[17-20]

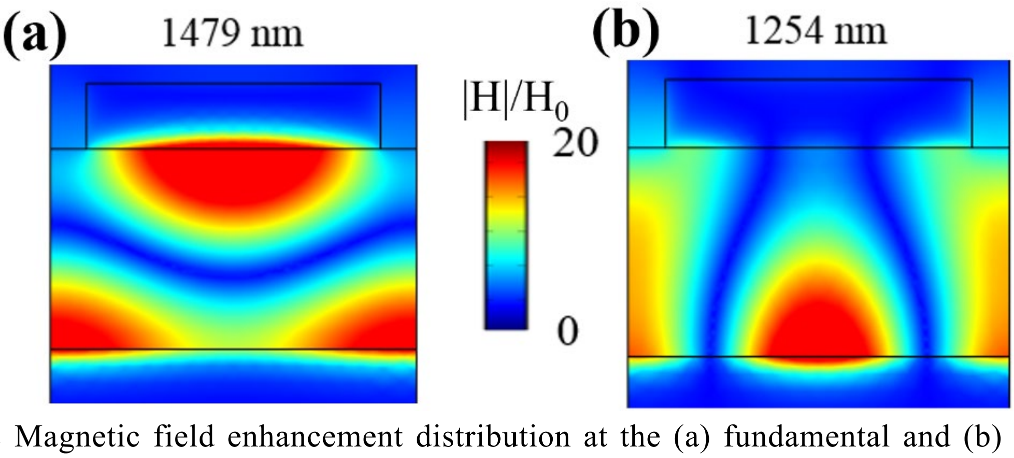

Fig. S2 Magnetic field enhancement distribution at the (a) fundamental and (b) higher-order resonances.

References

1. Wang, L., et al., *Nonlinear wavefront control with all-dielectric metasurfaces.* Nano Letters, 2018. **18**(6): p. 3978-3984.
2. Kruk, S., et al., *Nonlinear light generation in topological nanostructures.* Nature Nanotechnology, 2019. **14**(2): p. 126-130.
3. Carletti, L., et al., *Giant nonlinear response at the nanoscale driven by bound states in the continuum.* Physical Review Letters, 2018. **121**(3): p. 033903.
4. Koshelev, K., et al., *Subwavelength dielectric resonators for nonlinear nanophotonics.* Science, 2020. **367**(6475): p. 288-292.
5. Fedotova, A., et al., *Second-harmonic generation in resonant nonlinear metasurfaces based on lithium niobate.* Nano Letters, 2020. **20**(12): p. 8608-8614.
6. Johnson, P.B. and R.W. Christy, *Optical constants of the noble metals.* Physical Review B, 1972. **6**(12): p. 4370-4379.
7. Zelmon, D.E., D.L. Small, and D. Jundt, *Infrared corrected Sellmeier coefficients for congruently grown lithium niobate and 5 mol. % magnesium oxide-doped lithium niobate.* Journal of the Optical Society of America B-Optical Physics, 1997. **14**(12): p. 3319-3322.
8. Gangaraj, S.A.H., et al., *Broadband field enhancement and giant nonlinear effects in terminated unidirectional plasmonic waveguides.* Physical Review Applied, 2020. **14**(5): p. 054061.
9. Krause, D., C.W. Teplin, and C.T. Rogers, *Optical surface second harmonic measurements of isotropic thin-film metals: Gold, silver, copper, aluminum, and tantalum.* Journal of Applied Physics, 2004. **96**(7): p. 3626-3634.
10. Weismann, M. and N.C. Panoiu, *Theoretical and computational analysis of second- and third-harmonic generation in periodically patterned graphene and transition-metal dichalcogenide monolayers.* Physical Review B, 2016. **94**(3): p. 035435.
11. Dalstein, L., et al., *Nonlinear optical response of a gold surface in the visible range: A study by two-color sum-frequency generation spectroscopy. I. Experimental determination.* Journal of Chemical Physics, 2018. **148**(13): p. 134701.
12. Butet, J., et al., *Nonlinear Mie theory for the second harmonic generation in metallic nanoshells.* Journal of the Optical Society of America B-Optical Physics, 2012. **29**(8): p. 2213-2221.
13. Bachelier, G., et al., *Origin of optical second-harmonic generation in spherical gold nanoparticles: Local surface and nonlocal bulk contributions.* Physical Review B, 2010. **82**(23): p. 235403.
14. Bernasconi, G.D., J. Butet, and O.J.F. Martin, *Mode analysis of second-harmonic generation in plasmonic nanostructures.* Journal of the Optical Society of America B-Optical Physics, 2016. **33**(4): p. 768-779.
15. Reddy, K.N., et al., *Revisiting the boundary conditions for second-harmonic generation at metal-dielectric interfaces.* Journal of the Optical Society of America B-Optical Physics, 2017. **34**(9): p. 1824-1832.
16. Jin, B. and C. Argyropoulos, *Enhanced four-wave mixing with nonlinear plasmonic metasurfaces.* Scientific Reports, 2016. **6**(1): p. 28746.

17. Pors, A., M.G. Nielsen, and S.I. Bozhevolnyi, *Broadband plasmonic half-wave plates in reflection.* Optics Letters, 2013. **38**(4): p. 513-515.
18. Pors, A., M.G. Nielsen, and S.I. Bozhevolnyi, *Analog Computing Using Reflective Plasmonic Metasurfaces.* Nano Letters, 2015. **15**(1): p. 791-797.
19. Miao, Z., et al., *Widely Tunable Terahertz Phase Modulation with Gate-Controlled Graphene Metasurfaces.* Physical Review X, 2015. **5**(4): p. 041027.
20. Huang, Y.W., et al., *Gate-Tunable Conducting Oxide Metasurfaces.* Nano Lett, 2016. **16**(9): p. 5319-25.